A Volcano Rekindled: The Renewed Eruption of Mount St. Helens, 2004–2006
Edited by David R. Sherrod, William E. Scott, and Peter H. Stauffer
U.S. Geological Survey Professional Paper 1750, 2008

Chapter 5

Broadband Characteristics of Earthquakes Recorded During a Dome-Building Eruption at Mount St. Helens, Washington, Between October 2004 and May 2005

By Stephen P. Horton[1], Robert D. Norris[2], and Seth C. Moran[3]

Abstract

From October 2004 to May 2005, the Center for Earthquake Research and Information of the University of Memphis operated two to six broadband seismometers within 5 to 20 km of Mount St. Helens to help monitor recent seismic and volcanic activity. Approximately 57,000 earthquakes identified during the 7-month deployment had a normal magnitude distribution with a mean magnitude of 1.78 and a standard deviation of 0.24 magnitude units. Both the mode and range of earthquake magnitude and the rate of activity varied during the deployment. We examined the time domain and spectral characteristics of two classes of events seen during dome building. These include volcano-tectonic earthquakes and lower-frequency events. Lower-frequency events are further classified into hybrid earthquakes, low-frequency earthquakes, and long-duration volcanic tremor. Hybrid and low-frequency earthquakes showed a continuum of characteristics that varied systematically with time. A progressive loss of high-frequency seismic energy occurred in earthquakes as magma approached and eventually reached the surface. The spectral shape of large and small earthquakes occurring within days of each other did not vary with magnitude. Volcanic tremor events and lower-frequency earthquakes displayed consistent spectral peaks, although higher frequencies were more favorably excited during tremor than earthquakes.

Introduction

Two classes of earthquakes are commonly observed at volcanoes around the world. One class, termed volcano-tectonic (VT) earthquakes by Latter (1981), consists of high-frequency events with sharp, well-defined body-wave phases. Volcano-tectonic events are produced by shear failure in solid rock; their broadband seismic waveforms are indistinguishable from normal tectonic earthquakes (Chouet, 1996). The second class of earthquakes observed at volcanoes consists of lower-frequency events that are thought to originate from a boundary between a fluid, such as magma or gas, and the solid surrounding rock (see, for example, Neuberg and others, 2006).

In this study we follow the convention of Moran and others (this volume, chap. 2), dividing lower-frequency earthquakes into two groups, hybrid and low-frequency (LF) earthquakes. Low-frequency events have a weak high-frequency onset followed by a harmonic waveform with one to several dominant frequencies in the range of 0.5–5 Hz (Chouet, 1996). In LF events, the P wave is often emergent, and the S wave is often obscured. Hybrid events blend the characteristics of both the VT and LF events (Lahr and others, 1994). The onset of the hybrid earthquake shows more pronounced high-frequency energy than the LF event, whereas the coda of both types is dominated by a high-amplitude, low-frequency waveform (Chouet, 1996). First-motion polarities are often mixed for both VT and hybrid events, whereas LF events generally display the same polarity at all stations (Lahr and others, 1994).

A network of eight broadband seismometers was installed at Mount St. Helens in October 2004 (fig. 1) to record seismic activity associated with the dome-building eruption that began with seismic unrest on September 23. The Cascades Volcano Observatory (CVO) installed two broadband seismometers northwest of the Mount St. Helens crater in October 2004. The Center for Earthquake Research and Information (CERI) at

[1] Center for Earthquake Research and Information, University of Memphis, 3890 Central Avenue, Memphis, TN 38155

[2] U.S. Geological Survey, at Pacific Northwest Seismic Network, Department of Earth and Space Sciences, University of Washington, Box 351310, Seattle, WA 98195

[3] U.S. Geological Survey, 1300 SE Cardinal Court, Vancouver, WA 98683

the University of Memphis installed six temporary stations at complementary azimuths around the volcano to provide better coverage of the eruption at about the same time. The CERI stations were removed in May 2005, and a separate temporary broadband network, installed by the U.S. Geological Survey in May 2005, was operated until October 2005. This analysis covers only the time period of the first temporary deployment.

Moran and others (this volume, chap. 2) separated the seismic activity associated with the dome-building eruption at Mount St. Helens into two temporal phases. The first was the vent-clearing phase that began with a swarm of shallow VT earthquakes on September 23 and ended with an explosion on October 5. A gradual transition from the VT events to lower-frequency earthquakes occurred between September 25 and October 1. This transition from VT to lower-frequency earthquakes was not recorded with broadband seismometers, because the first broadband seismometer was installed by CVO at Johnston Ridge Observatory (JRO; fig. 1) on October 1, 2004, about 1600 PDT. After October 5, seismicity was dominated by lower-frequency earthquakes. Tens of thousands of lower-frequency earthquakes were recorded by the broadband network between then and May 2005, with just one high-frequency (VT) earthquake. A few episodes of volcanic tremor were also observed, mostly before the CERI component of the broadband network became operational (Moran and others, this volume, chap. 2).

Lower-frequency earthquakes at Mount St. Helens were observed in association with eruptions in the 1980s (see, for example, Endo and others, 1981; Malone, 1983; and Malone and others, 1983). Those events were recorded using short-period, vertical-component seismometers. Since the mid-1990s, broadband seismometers have been used to record earthquakes and volcanic tremor on numerous volcanoes around the world, but the broadband recordings discussed here were the first at Mount St. Helens.

Because hybrid and LF earthquakes form the bulk of the signals recorded during the CERI broadband deployment, our analysis focuses on those events. We examine aspects of the seismicity that can be addressed by continuous, broadband, and unclipped recordings of the earthquakes. Following a brief description of the temporary broadband seismic network at Mount St. Helens, we discuss our search of the dataset for very

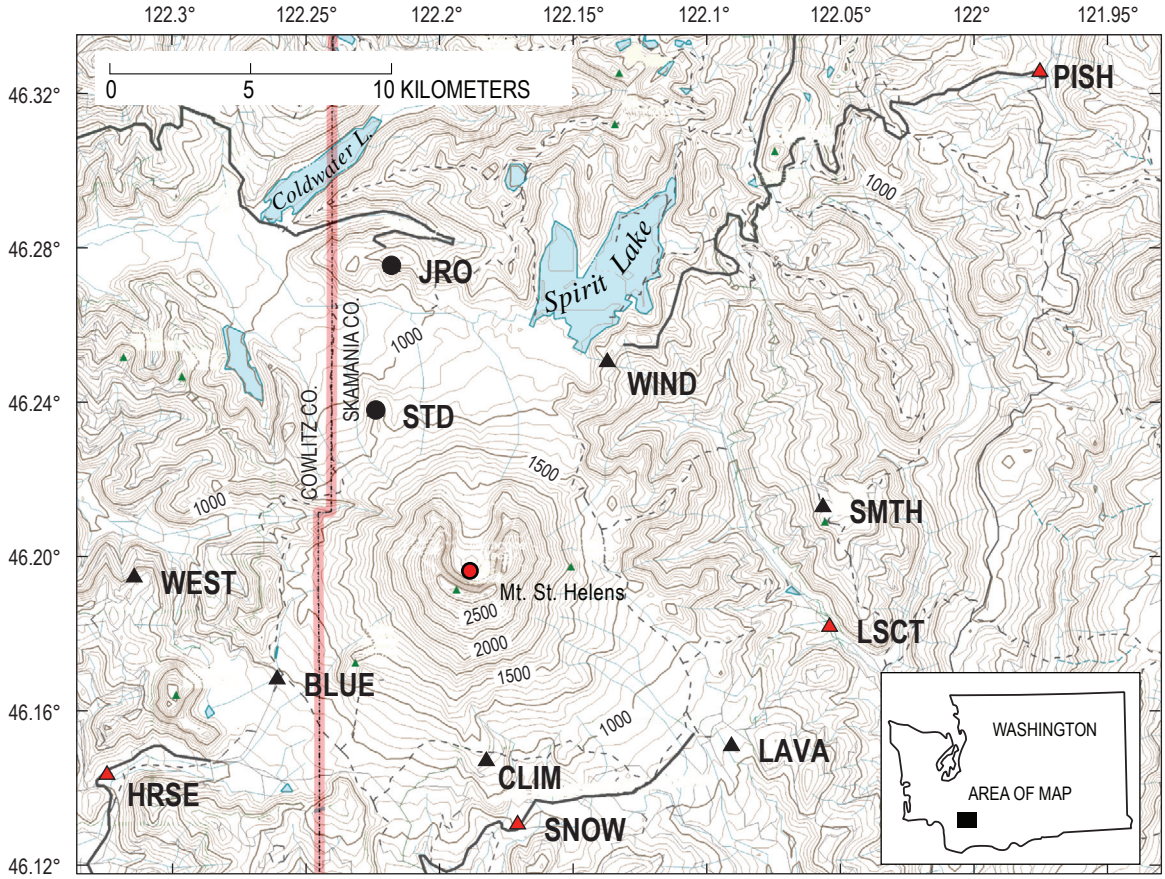

Figure 1. Broadband seismic stations at Mount St. Helens used in this study (from table 1). Black circles indicate location of CVO broadband seismometers. Black triangles indicate initial locations of CERI broadband seismometers. Red triangles show four CERI instruments redeployed to lower altitudes in early December 2004 to allow servicing throughout winter. Red circle indicates centroid of seismic activity. Roads shown in black; dashed lines are trails. Contours in meters, contour interval 50 m.

long period (VLP) pulses as described by Almendros and others (2002). We examine the variation in the rate and the magnitude distribution of the events identified by our trigger algorithm. We then look at the differences and similarities between hybrid and LF earthquakes and test a numerical measure of event character. Finally some issues are discussed related to wave propagation that make it difficult to determine focal mechanisms for these events through waveform modeling.

Broadband Network

Broadband seismic monitoring at Mount St. Helens began with CVO's installation of a Guralp CMG-6TD at JRO on October 1, 2004, approximately 1 week after the onset of increased seismic activity at the volcano (fig. 1). CVO installed a second instrument at Studebaker Ridge (STD) on October 5. Telemetry for both sites was established in late October, providing real-time broadband monitoring of Mount St. Helens seismicity (McChesney and others, this volume, chap. 7). On October 3, CERI, in cooperation with CVO and the Pacific Northwest Seismic Network (PNSN), began deploying broadband instruments with onsite recording capability. Station locations were chosen to provide the optimum azimuthal coverage, encircling the vent at the closest possible distance to Mount St. Helens. Budget, safety, and logistical considerations limited us to road-accessible sites. We deployed six Guralp CMG-6TD broadband seismometers within about 5 to 10 km of the seismic activity by October 5 (fig. 1). Four strong-motion instruments (Kinemetrics Altus K2 Recorder) were also deployed, although earthquakes in the sequence did not trigger the latter instruments.

A typical broadband station had a Guralp CMG-6TD sensor buried in a hole about 18 inches deep. Timing was provided by a GPS antenna. Power was provided by 12-V batteries recharged by a 30-W solar panel on a 1.2-m-tall stand. The broadband seismometers recorded three channels continuously at 50 samples per second and had a flat response to ground velocity between 0.033 and 25 Hz. Data were stored onsite using 2 GB of internal flash memory. With reasonable data compression, and a few sunny days for solar-power recharge, a service interval of 6 to 8 weeks was adequate to ensure no loss of data. In late October we started removing several temporary stations located in remote settings to avoid having them snowed under for the winter (table 1). By early November only two of the temporary stations, BLUE and LAVA, remained. Fortunately, these stations were southwest and southeast of the volcanic crater, so they, along with the two CVO stations, still provided reasonable azimuthal coverage. At the beginning of December, we moved stations to sites where the anticipated snow depth would not exceed 2.4 m. Three of these sites were winter recreational Sno-Parks maintained by the U.S. Forest Service, with plowed road access during normal snow years. The fourth site, LSCT, was sufficiently low in altitude to be accessible year-round.

Very Long Period Seismicity, October-November 2004

One of the principal reasons for our rapid deployment of broadband seismometers was to record any very long period (VLP) seismicity associated with the eruption that would otherwise have been missed by the PNSN short-period stations. We looked for evidence of VLP signals as described by Almendros and others (2002) in the period range 5–30 s. A moving root-mean-squared (RMS) average applied to bandpass-filtered seismograms was helpful in identifying trends and potential pulses. We checked peaks and trends observed in the moving average by visual inspection of the time series. For example, a moving RMS average was computed from seismograms recorded from October 5 through October 8 (fig. 2*A*). The two large peaks observed at station WIND in figure 2*A* at about 1600 (PDT) on October 6 and 0200 on October 8 can be correlated with spikes at other stations in the network. The first peak was produced by surface waves following a shallow M_w 6.2 earthquake that occurred in Indonesia at 1531 (PDT) on October 6. The second large peak was produced by body and surface waves following a shallow M_w 6.8 earthquake that occurred in the Solomon Islands at 0127 on October 8.

Two broad increases in RMS levels occurred between October 7 and 9. These trends were too broad to be teleseismic arrivals or VLP pulses but could have been caused by very long duration resonance of the volcano's magmatic-hydrologic system. We computed the RMS average at station LON, approximately 68 km north of Mount St. Helens and found that the broad trend increases observed at WIND, only 7.15 km from the vent, were matched by concurrent increases at LON, which suggests the source of the increase may be regional. Seismic waves that emanated from a local source below the Mount St. Helens crater should have attenuated with distance. To investigate amplitude as a function of distance from the crater, we plotted seismograms from October 7 to 9 arranged by the station distance from the crater (fig. 2*B*). The peak amplitudes and general character of the waveforms were similar at all stations, including LON. Because attenuation was not evident, we concluded that the broad energy increases did not result from a local source below the Mount St. Helens crater, but rather from a regional source. The increased long-period energy is best explained as seismic noise (microseisms) generated by a low-pressure weather system that approached the Pacific Northwest coast on October 7 and remained in the coastal area during the following 3 days. Microseisms, a nearly harmonic modulated waveform with periods around 6 s, have long been associated with storms over water, including normal low-pressure systems. Longuet-Higgins (1950) showed that the interaction of water waves with similar periods and different directions generates pressure waves that efficiently couple with the solid earth to produce seismic surface waves. These surface waves can propagate with gradual loss of energy over broad areas of the continent.

Table 1. Broadband station locations and dates of operation.

[Stations JRO and STD operated by Cascades Volcanic Observatory; others installed by Center for Earthquake Research and Information as part of this report. Datum is WGS84. Altitude is orthometric, interpolated from topographic maps after plotting locations. Distance is measured from centroid of seismic activity, the surface trace of which approximates the position of the vent.]

Station	Latitude (N)	Longitude (W)	Altitude (m)	Distance from vent (km)	Dates of operation
JRO	46.2751	122.2178	1,290	8.98	10/01/04–08/10/06
STD	46.2376	122.2240	1,250	5.28	10/25/04–present [1]
WIND	46.2504	122.1372	1,230	7.15	10/03/04–10/31/04
LAVA	46.1509	122.0908	850	9.13	10/03/04–12/02/04
BLUE	46.1682	122.2608	980	6.41	10/03/04–12/02/04
WEST	46.1946	122.3143	1,120	9.66	10/04/04–11/01/04
CLIM	46.1470	122.1825	1,140	5.58	10/04/04–11/01/04
SMTH	46.2128	122.0566	1,090	10.34	10/05/04–10/27/04
LSCT	46.1818	122.0540	500	10.52	12/03/04–05/07/05
SNOW	46.1306	122.1708	810	7.51	12/04/04–05/07/05
HRSE	46.1434	122.3244	620	12.02	12/05/04–05/06/05
PISH	46.3256	121.9754	860	21.77	12/07/04–05/08/05

[1] As of March 17, 2008.

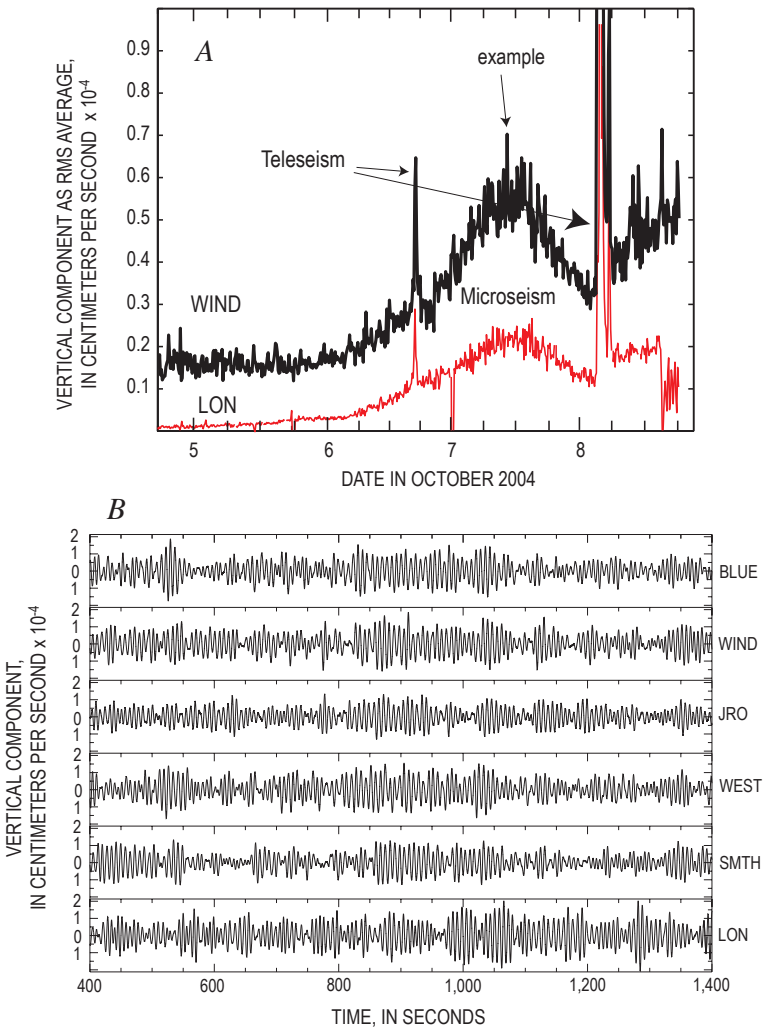

Figure 2. Ground motion recorded at Mount St. Helens, October 5–8, 2004. *A*, Moving RMS average (over consecutive 600-s window) of filtered (5–30 s) vertical component data at station WIND (black) and Pacific Northwest Seismic Network broadband station LON (red). Data from LON plotted in counts but scaled for visual comparison with velocity data from WIND. Date on x axis marks start of each day, PDT. Concurrent large sharp peaks at both stations are teleseismic arrivals. Broad increase that peaks about midday October 7 was most likely due to weather system impinging on region. Arrow labeled "example" shows approximate time displayed in bottom figure. *B*, Vertical component seismograms, all scaled to same absolute amplitude, for ~16-minute interval of intense low-frequency energy as recorded at six stations (listed at right edge).

Visual inspections of all moving RMS average peaks occurring in October and November 2004 revealed no VLP signals that originated below the Mount St. Helens crater. The absence of observed VLP signals could have been due in part to the distance of our stations from the source. Rapid decay of signal amplitude with distance is considered characteristic of VLP signals (Almendros and Chouet, 2003). VLP signals have been observed at other volcanoes at distances of less than 5 km (for example, Almendros and others, 2002; Aster and others, 2003). The closest broadband stations recording during the first deployment were STD and CLIM, about 5.28 km and 5.58 km respectively from the centroid of seismicity (fig. 1). Thus we cannot definitively rule out the occurrence of VLP signals at Mount St. Helens during this time period.

October 2004–May 2005 Seismicity Recorded by the Broadband Network

Event Magnitudes and Rates

Thousands of earthquakes were recorded during the 7-month broadband network deployment at Mount St. Helens. Because our data were not recorded in trigger mode, we developed a trigger algorithm based on the ratio of short-term (0.2 s) and long-term (320 s) averages to isolate individual events from the continuous records. We first applied a 0.5–3-Hz bandpass filter to the data and then used a short-term to long-term trigger ratio of 6 to identify 57,635 events. We assigned a magnitude for each event on the basis of the peak velocity (*pv*) measured on the vertical component at each CERI station. The body-wave arrivals of both hybrid and LF events were of smaller amplitude than the low-frequency waveforms that followed, so we assumed *pv* to be a surface-wave amplitude. We therefore adjusted the measured *pv* by the square root of the distance from the centroid of seismicity to the station (table 1) to account for geometrical spreading. The centroid location, 46.1964ºN and 122.18882ºW, was calculated from the PNSN catalog for events with $M_d \geq 2.5$ during this time period. The magnitude was given by $M_S = \log_{10}(pv) + 5.78$, where the distance-adjusted *pv* was averaged over all CERI stations and the constant (5.78) was calculated so that the largest event had M_S 3.4, equal to the PNSN duration-magnitude estimate for that event. Our magnitude estimates were reasonably consistent with PNSN magnitudes for events above M_d 2.6.

Figure 3*A* shows the distribution of event magnitudes selected by our trigger algorithm for the entire period of the network deployment. These have a normal distribution, with mean magnitude (M_S) of 1.78 and a standard deviation of 0.24 magnitude units. When comparing event triggers to the continuous seismograms, we observed that small earthquakes occurring in the coda of larger events were not likely to be selected by our trigger algorithm. Therefore, the distribution of smaller earthquakes in the sequence is probably not well characterized. The distribution of larger events, however, is probably well characterized. The distribution of earthquake size and the rate of activity varied with time, with larger earthquakes occurring irregularly throughout the sequence. To help discern patterns, we divided the entire dataset into 24-hour segments, calculated the magnitude distribution of each time interval as in figure 3*A*, and contoured the resulting magnitude distributions over time (fig. 3*B*). Most of the events with $M_S \geq 3$ occurred before October 5 and were associated with the closing days of the vent-clearing phase (Moran and others, this volume, chap. 2). The rate of seismic activity was quite high at that time, and the distribution of earthquake sizes was bimodal, with peaks around M_S 2.5 and M_S 2 and a range slightly greater than 2 magnitude units.

After October 5 the rate of seismic activity slowed drastically and the modal event size decreased to M_S 1.7 (fig. 3*B*). The minimum event size also increased to about M_S 1.5 from a minimum M_S of ~1.0 during the more active vent-clearing

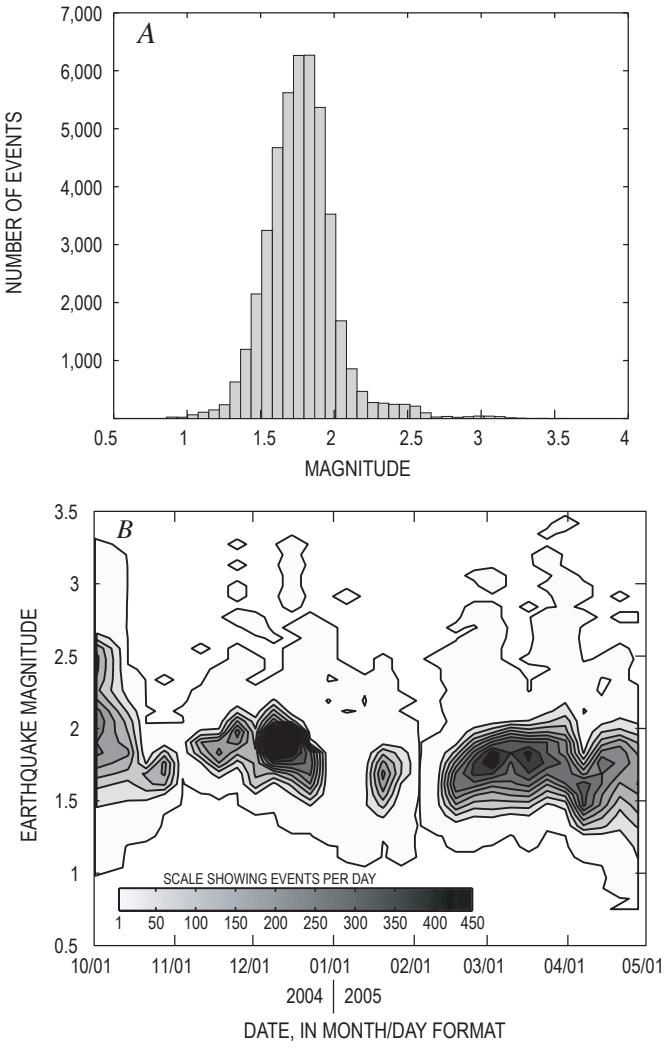

Figure 3. Event-magnitude occurrence for the more than 57,000 earthquakes identified during this deployment. Magnitudes are binned in 0.072-magnitude intervals. *A,* Histogram showing magnitude distribution. *B,* Time-series plot showing magnitude distribution. Contour interval is 50 events per day.

period. Because the trigger algorithm should have been more sensitive to small events when the rate of larger events was low, this increase of minimum event size during a period of reduced seismic activity suggests that the observed distribution for small events was not entirely due to lack of detection. Instead, small events were simply not plentiful during some time intervals.

Both the range and mode of earthquake size and the rate of seismic activity increased through the latter part of November 2004. These increases coincided with the approach and collision of spine 3 with the south crater wall (Schilling and others, this volume, chap. 8; Vallance and others, this volume, chap. 9). The seismic activity continued at a high rate through the middle of December, when 10 events with $M_S \geq 3.0$ occurred between December 17 and 19. Subsequently, both the rate of seismic activity and the modal size of events began to decrease. This trend continued through the middle of January, as spine 3 was disintegrating and being shoved aside by spine 4, and a large explosion occurred on January 16, 2005 (Moran and others, this volume, chap. 6). The seismicity rate increased through the latter part of January 2005. The small number of events between January 29 and February 6 was artificial, reflecting a loss of network data during that time interval. The seismicity rate remained high in March and April, when 14 $M_S \geq 3.0$ events occurred. It appears that the sporadic occurrence of events of $M_S \geq 3.0$ coincided with intervals of high seismicity rates.

Characteristics of Lower-Frequency Earthquakes at Mount St. Helens

Since the mid-1990s, broadband seismometers have been used to record earthquakes and tremor on numerous volcanoes around the world. Because our data were the first broadband recordings at Mount St. Helens, we looked with special care at the broadband character of the events recorded on our network. We recorded one high-frequency tectonic earthquake, two episodes of volcanic tremor, and thousands of lower-frequency earthquakes during the deployment. In this section we describe the characteristics of the lower-frequency events and compare our observations to the reported features of earthquakes observed at other volcanoes.

The first step was to compare a lower-frequency event to the high-frequency tectonic earthquake, because these form the two main types of earthquakes recorded at volcanoes (see, for example, Latter, 1981). We did not record volcano-tectonic events associated with the vent-clearing phase, because the broadband seismometers were only installed at the close of that phase. However, a small local tectonic event was recorded on November 22, 2004, at 0853 PST. Figure 4 shows seismograms and their associated spectra for that tectonic earthquake and an example LF earthquake, M_S 3.3, recorded on November 27, 2004, at 0601 PST. The tectonic event was not located by PNSN. However, a local hypocenter is required by the short S-P arrival-time differences at stations LAVA (1.5 s) and BLUE (2 s). We consider the event to be tectonic because it had sharp and well-defined P and S phases followed by a short high-frequency coda. Peak energy for this event was between 5 and 12 Hz, with very low spectral levels at frequencies less than 5 Hz. By contrast, the LF event had a low-amplitude onset, with frequencies as high as about 10 Hz, followed by a strong, long-duration, and lower-frequency waveform. The spectrum had significant energy between 0.3 and 5 Hz, with multiple spectral peaks suggestive of harmonic motion as observed for lower-frequency earthquakes at other volcanoes (for example, Chouet, 1996; Neuberg and others, 2006).

Next we compare the hybrid and LF earthquakes that form the two types of lower-frequency earthquakes recorded during the first year of renewed eruption at Mount St. Helens (Moran and others, this volume, chap. 2). For example, figure 5*A* shows the broadband seismograms for a M_S 3.13 hybrid earthquake recorded on October 3, 2004, at 1812 (PDT) and a M_S 3.2 LF earthquake recorded on November 28, 2004, at 1807 (PST). Figure 5*B* shows the same seismograms after 7-Hz highpass filters were applied, and figure 5*C* shows the Fourier displacement spectra for both events. The broadband waveforms of both events are dominated by the lower-

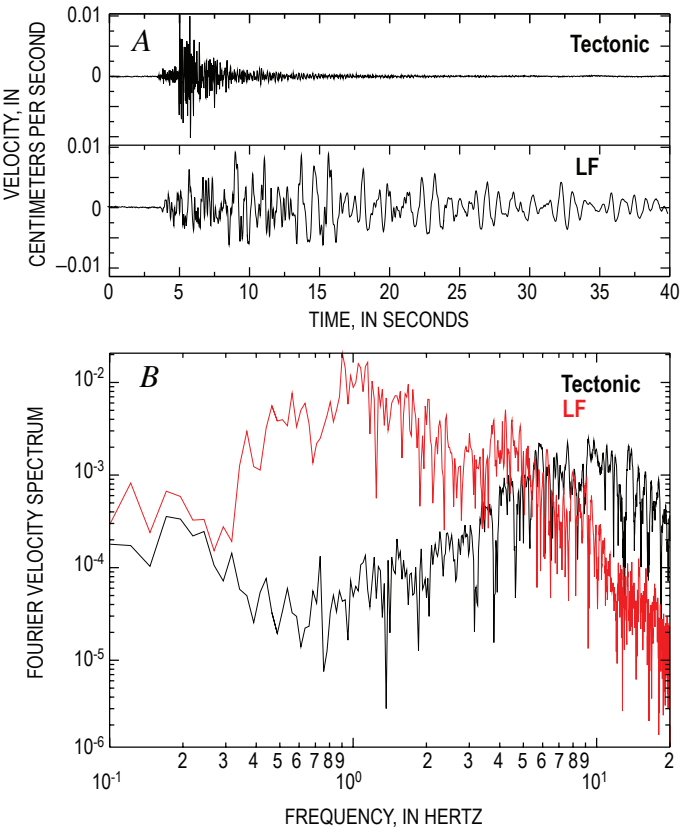

Figure 4. Seismograms and spectral characteristics for tectonic earthquake recorded November 22, 2004, and a low-frequency earthquake recorded November 27, 2004. *A*, Comparison of seismograms from station LAVA, plotted at same absolute scale. *B*, Fourier velocity spectra of associated seismograms. Tectonic earthquake is black trace; low-frequency event is red trace.

frequency (from 0.3 to about 5 Hz), nondispersive waves that give rise to the name of this class of earthquake. At frequencies between 0.3 and 2.0 Hz, the spectral amplitudes of the LF event slightly exceed those of the hybrid event (consistent with the slightly larger magnitude estimate), whereas at frequencies above 3.0 Hz, the spectral amplitudes of the hybrid event exceed the LF spectral amplitudes. This difference in high-frequency energy is also apparent in the time series, where the hybrid earthquake has a much more pronounced high-frequency onset (fig. 5*A*).

This difference in high-frequency energy is the primary difference between hybrid and LF earthquakes. It may result from a difference in the earthquake source process or a difference in the rock along the path from source to receiver that affects wave propagation (an increase in attenuation related to a reduction in source depth, for example). To investigate these possibilities, we filtered the lower-frequency energy from the signal. The filtered records (fig. 5*B*) show that both events actually have a high-frequency onset, although the amplitude is about five times larger for the hybrid event. Further, the high-frequency component of both events is similar in form and of comparable duration, extending well into the low-frequency waveform. This similarity in form and duration indicates that attenuation near the earthquake sources and along the paths to the receiver did not differ significantly. Rather, more high-frequency energy was generated at the source for the hybrid than for the LF earthquake. This is consistent with a larger component of shear faulting during the hybrid earthquake.

We explored the similarity in spectra between small and larger events in figure 6, where the velocity spectrum of the M_S 3.1 hybrid event (October 3, 2004) was compared to a randomly chosen M_S 1.7 event that occurred on October 11, 2004. The spectrum of the M_S 1.7 event was multiplied by a factor of 20 in order to compare the shape of the spectra of both events. The spectrum of the smaller event disappears into the background noise and is undetectable above 10 Hz and below 0.5 Hz. Between 0.5 and 10 Hz, the spectra of the large and small events were quite similar in shape and amplitude. The similarity in spectral shape suggests that both the source and path were similar for the two events. For tectonic earthquakes, the peak in the velocity spectrum would be expected to shift to lower frequencies as rupture zone size increased for larger earthquakes (Brune, 1970). The consistency in the frequency range of the peak of spectral energy for different-size earthquakes favors models such as that of Chouet (1996), in which a pressure transient resonates in a crack of constant dimension (a few centimeters in width), or that of Neuberg and others (2006), in which brittle failure of magma provides seismic energy that resonates in a conduit section of constant dimension (~30 m wide and several hundred meters long). In both cases the amplitude of the resonance would be determined by the strength of the pressure transient or size of the brittle failure, whereas the shape of the spectrum would be constrained by the size and properties of the resonator.

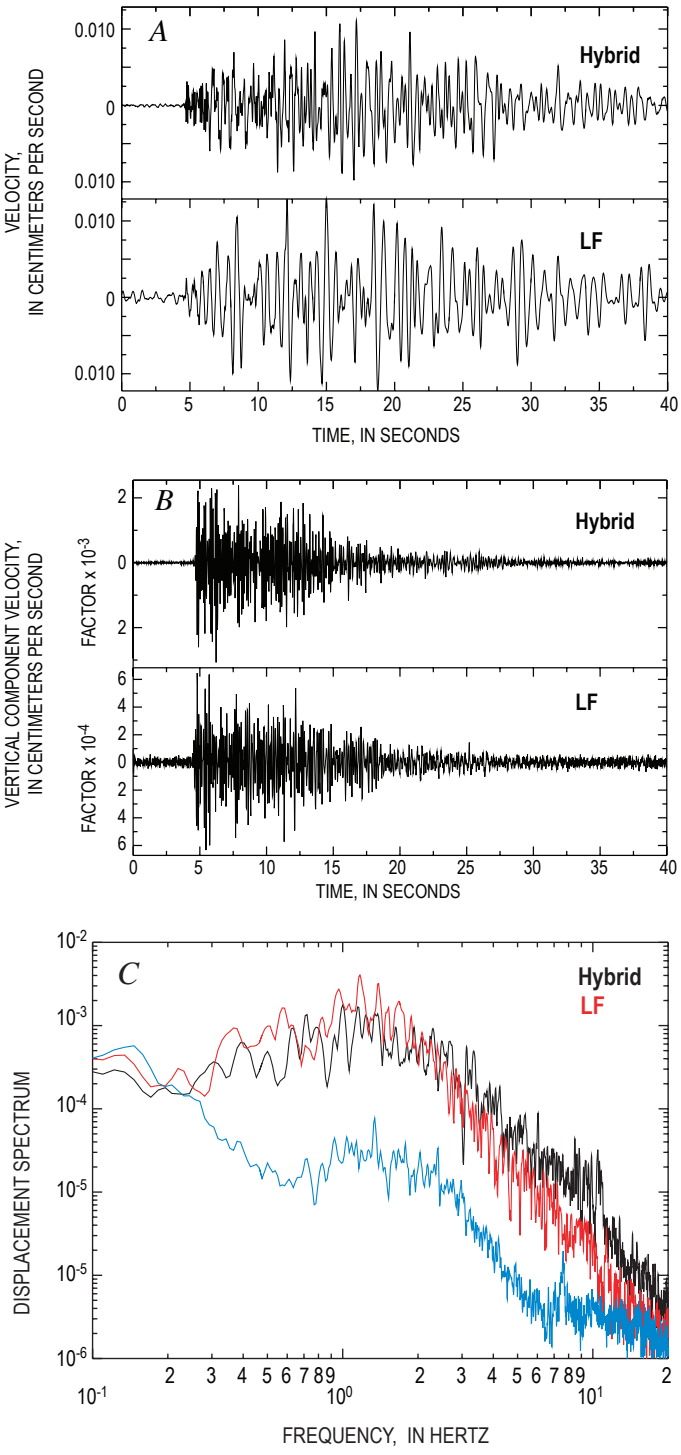

Figure 5. Comparison of seismic data from station BLUE for hybrid and low-frequency (LF) earthquakes. *A*, Vertical-component seismograms, plotted at same absolute scale. *B*, Corresponding 7-Hz highpass-filtered seismograms; note different scales. Decay of the waveforms is remarkably similar. *C*, Fourier displacement spectra of the original hybrid (black) and LF (red) seismograms. Spectrum of a 60-s interval from a "quiet" period on November 1, 2004, shows representative background noise level (blue). (This interval chosen because time intervals just before the two earthquakes contain the coda of other earthquakes.)

Resonance in a crack or conduit of constant dimensions produces amplitude spectra with strong peaks resulting from the summation of waves propagating between the boundaries of the structure. The specific frequencies of resonance are determined by the dimensions of the structure and the properties of the material within the conduit or crack. Identifying the frequencies of resonance would therefore place useful constraints on the volcanic process. Any given station can have a variety of peaks derived from its own particular source-receiver path and local site conditions, but the resonance peaks associated with a symmetric conduit or crack should be common to spectra observed at all stations independent of azimuth and distance. By comparing spectra at all stations, it should simply be a matter of identifying the common peaks.

A feature of the seismicity associated with this eruption of Mount St. Helens was the prominence of earthquake multiplets having highly similar waveforms (Thelen and others, this volume, chap. 4). Figure 7 shows the Fourier velocity spectra at six stations for a multiplet of 29 lower-frequency events ($2.1 \leq M_S \leq 2.2$) that occurred on October 16, 2004. The velocity spectra were normalized and overlaid for each station so that peaks that are consistent from event to event tend to stand out. Each station exhibits several consistent peaks in the range 0.4–2 Hz, but no peak appears consistently at all stations to indicate a specific frequency of source resonance. This lack of identifiable frequencies of source resonance is inconsistent with the resonance of a structure with simple geometry such as the rectangular crack of the Chouet (1996) model and the rectangular conduit of the Neuberg and others (2000) model. It suggests instead that wave propagation dominated the response at a given station and that source harmonics played a minor role. Alternatively, one can appeal to the excitation of a more complex, perhaps asymmetric, structure, where the harmonic response observed at a given station depends upon its location relative to the orientation of the source structure.

Fehler (1983) analyzed short-period records of tremor at Mount St. Helens that accompanied eruptions on August 7 and October 16–18, 1980. He found that the spectra of lower-frequency earthquakes were very similar to volcanic tremor, and he suggested that tremor was composed of many lower-frequency events inseparable in time. Neuberg and others (2000) observed that many episodes of volcanic tremor at Soufrière Hills volcano in Montserrat, West Indies, followed swarms of lower-frequency earthquakes in which the rate of earthquake occurrence continually increased until they merged into tremor. Figure 8*A* shows a seismogram with lower-frequency earthquakes followed by 58 minutes of volcanic tremor at Mount St. Helens on October 2, 2004. In this case, the lower-frequency earthquakes appeared to be distinct events occurring before and again after the volcanic tremor. There is no evidence to suggest that individual earthquakes merged to generate the volcanic tremor. Figure 8*B* shows the normalized velocity spectrum of one lower-frequency event and a 60-s window from the volcanic tremor. Neither spectrum displayed harmonic peaks at whole-number multiples of fundamental

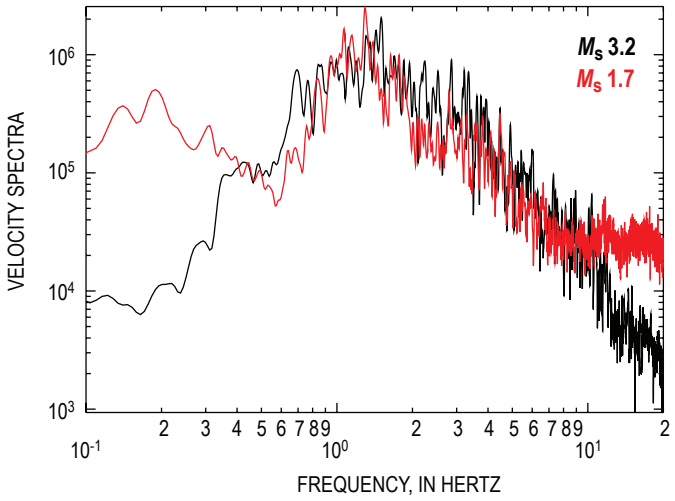

Figure 6. Spectral shapes of large and small events. Vertical-component Fourier velocity spectra recorded at station BLUE are shown for a M_S 3.2 hybrid event (black) and a randomly chosen M_S 1.7 event (red) occurring close together in time. Spectra of the small event (scaled up by a factor of 20) and large event are similar in shape between 0.5 and 10 Hz.

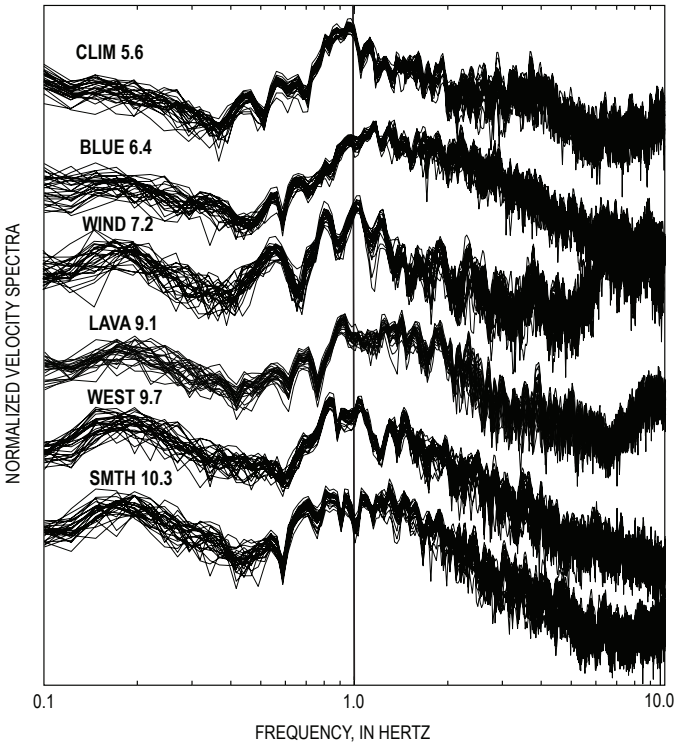

Figure 7. Comparison of spectra from six stations to identify source peaks. Fourier velocity spectra are plotted for a multiplet of 29 lower-frequency events ($2.1 \leq M_S \leq 2.2$) that occurred October 16, 2004. Velocity spectra are normalized and overlaid for each station so that peaks consistent from event to event become prominent. The distance to vent (see table 1) is to right of each station name.

frequencies. Both spectra had distinct peaks in common (for example, 0.8 and 1.1 Hz), consistent with Fehler's (1983) observations. However, the lower-frequency earthquake spectrum had a prominent peak at 0.6 Hz that was not observed in the spectrum of the volcanic tremor. This lower-frequency peak would be consistent with resonance of a structure having a larger dimension or with favorable excitation of the longer dimension of the same structure.

The progression from primarily volcano-tectonic events at the beginning of the 2004 eruption to combined hybrid and low-frequency (LF) events, then to dominantly LF events, reported by Moran and others (this volume, chap. 2), suggests a progressive loss of high-frequency seismic energy as magma moved toward and eventually onto the surface. Malone and collaborators have pointed out that gradual changes in event character were observed in many precursory swarms preceding dome-building eruptions at Mount St. Helens in the 1980s (Malone, 1983; Malone and others, 1983). During the 1980–86 dome-building eruptions, this transition became a diagnostic tool to predict eruption onset time (Malone and others, 1983; Swanson and others, 1983; Swanson and others, 1985). The high-frequency spectral difference between hybrid and LF events observed in figure 5*C* suggests that the slope of the high-frequency falloff could provide a measure to track the loss of high-frequency energy through time. To investigate this, the power spectra of an example hybrid and example LF event are compared in figure 9. Lines were fit by least squares to the high-frequency spectral amplitudes in the range 1–10 Hz. The slope of each line quantifies the rate of spectral amplitude decay with frequency or the high-frequency falloff of the velocity spectrum. The slope of the fitted line was −2.6 for the hybrid event and −4.9 for the LF event, indicating that this slope is a useful measure to quantify the high-frequency earthquake character.

We computed the high-frequency falloff for all events between October 4 and December 1, 2004 (CERI network station locations changed after December 1). Figure 10*A* shows earthquake magnitude versus time. Those events with magnitude in the range 1.5–2.0 are plotted in black, and other magnitudes are plotted in red. Because the high-frequency falloff could have a magnitude bias, the high-frequency falloff is plotted versus time (fig. 10*B*) with this same color convention. The slope of the high-frequency falloff ranged from approximately −1.75 to −5, defining a continuum between the ideal hybrid and LF events such as observed at Montserrat by Neuberg and others (2000). In early October, the slope values ranged from about −1.75 to −3.5, regardless of magnitude. The range was somewhat narrower for events with magnitude 1.5–2.0. Over time the slope values

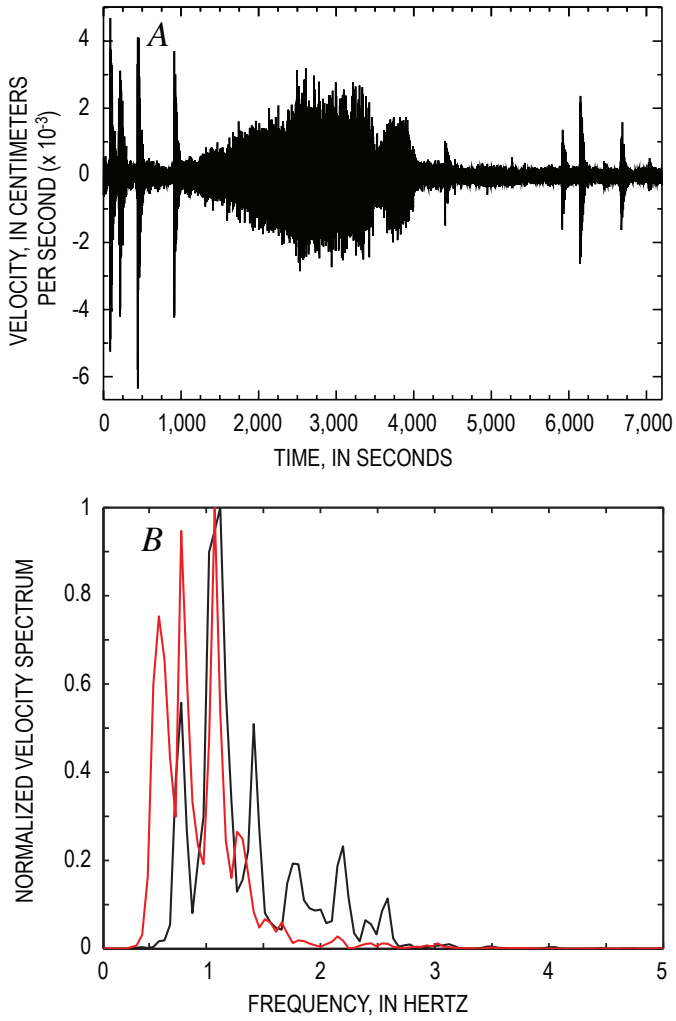

Figure 8. Seismic data showing 2-hour sequence of tremor recorded October 2, 2004, at JRO broadband station. *A*, Seismogram showing north component. Record of tremor is punctuated by impulsive earthquakes of lower-frequency type. *B*, Normalized velocity spectra for a lower-frequency earthquake (red) and the volcanic tremor (black) of October 2.

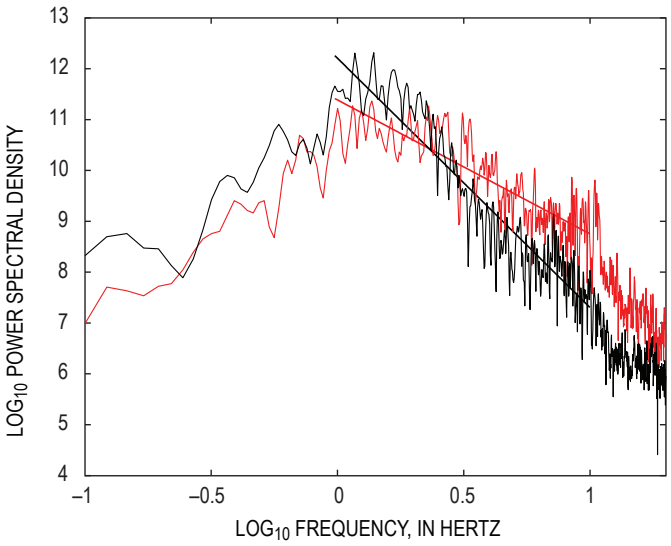

Figure 9. Power spectra of the vertical velocity components of a hybrid event (red) and a low-frequency event (black). Lines are least-squares fit to spectral amplitudes between 1 and 10 Hz; slopes are –2.6 for hybrid event and –4.9 for the LF event.

decreased to between about −3 and −4 at the end of October. The slope values continued at this level or decreased slightly until the end of November. If we arbitrarily declared a slope of −3.0 as the dividing line between hybrid and LF, then this figure would suggest about a 4:1 ratio of hybrid to LF events occurred between October 4 and October 5, decreasing smoothly to a 1:1 ratio by October 10, and decreasing to a 1:4 ratio by October 17. Other than a small increase around October 20, the slope continued to decrease so that by October 24, around 95 percent of the events were low frequency.

The gradual decrease in the slope of the high-frequency falloff over time reflects a progressive loss of high-frequency seismic energy. The loss of high-frequency seismic energy coincides with magma approaching and reaching the surface on October 11 (Scott and others, this volume, chap. 1). This lessening of high-frequency energy could be related to a decrease in earthquake source depth, with near-surface heterogeneity and anelasticity serving to filter out the higher-frequency parts of the seismograms. Alternatively, it may be related to a decrease in the static stress drop accompanying frictional slip as the magma plug, which initially needed to force its way through overlying rock, met with less resistance after the path to the surface was cleared.

Waveform Modeling

The record section in figure 11*A* shows bandpass-filtered (0.1–1 Hz) seismograms for a *M*s 2.9 LF earthquake that occurred on March 1, 2005, at 0928 PST. For this event, the acceleration record at station SEP in the crater was available. The SEP record was substantially clipped, but the filtered record should still illustrate the general character of ground acceleration in this passband. This earthquake was assigned a depth of 0.4 km by the PNSN. The seismograms all exhibited a low-amplitude onset followed by a long-duration, low-frequency waveform even at the closest station (SEP) recording acceleration. Signal duration increased with distance, from 15–20 s at less than 1 km epicentral distance from the source to ~50 s at 20 km distance. The first onset of larger-amplitude arrivals propagated at roughly 2 km/s. To investigate particle motion we chose a 6-s window having

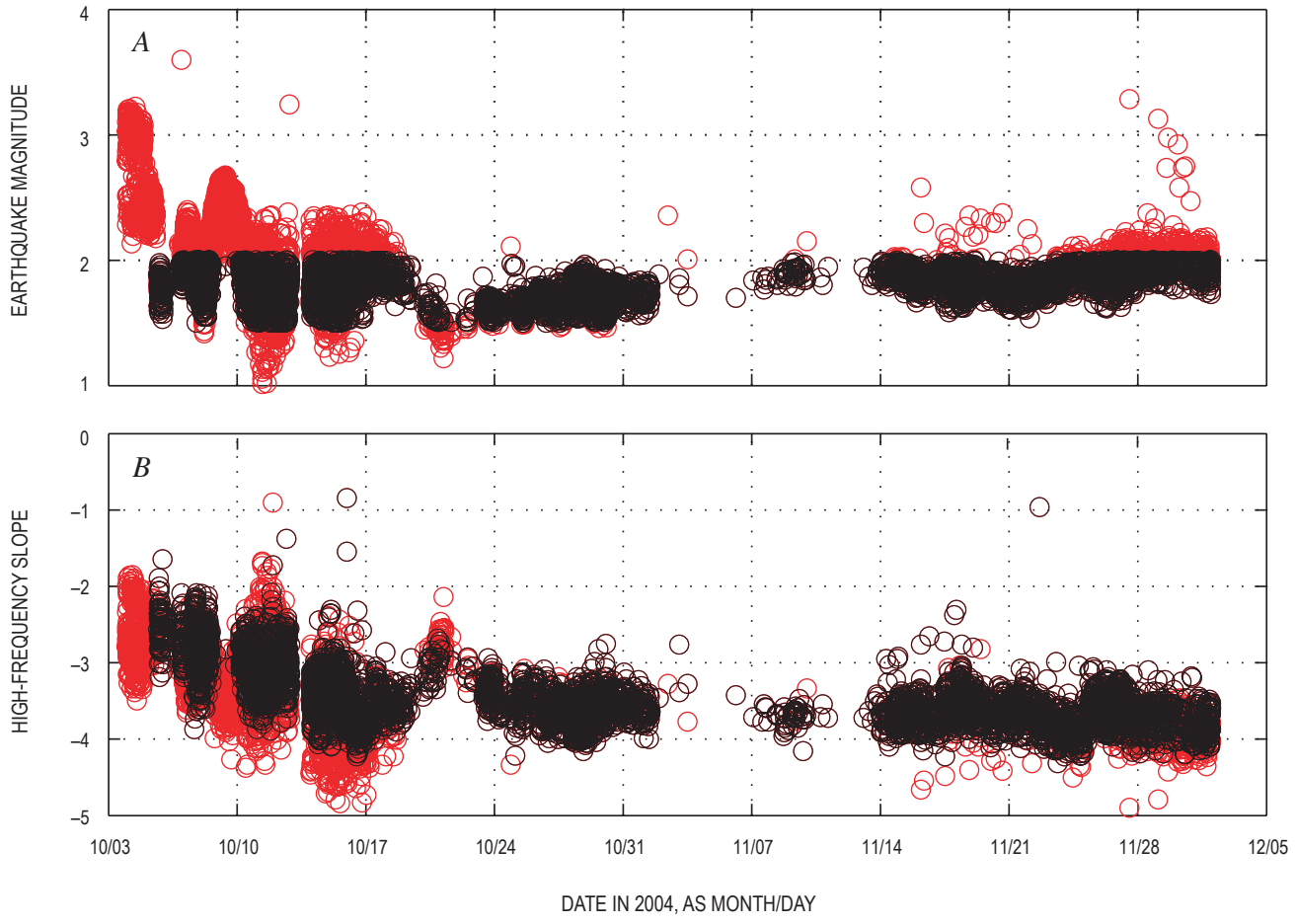

Figure 10. Time series showing seismic data from station BLUE. *A*, Magnitude versus time. Black circles show events in the range $1.5 \leq M_s \leq 2.0$; red circles are all other events. *B*, Plot of high-frequency slope versus time. Symbol color is determined by magnitude as in *A* (black circles, $1.5 \leq M_s \leq 2.0$).

a group velocity of 2 km/s for each station. At station PISH the particle motion in the vertical-radial plane was retrograde elliptical motion, characteristic of Rayleigh waves. However, the transverse component also had significant energy in this window, indicative either of Love waves or of multipathing. For the closer stations, the particle motion in the vertical-radial plane was more complex, suggesting interaction of body and surface waves in this window.

We used a reflection matrix method (Randall and others, 1995) to compute synthetic seismograms for a one-dimensional (1D) velocity model. The velocity model (table 2) was modified from the P-wave velocity model of Lees and Crosson (1989). The S-wave velocity in each layer was calculated from the P-wave velocity using a ratio of 1.7, based on the work of Sudo and Kong (2001), who found an average V_P / V_S ratio of 1.704 fit observed P- and S-wave travel times at all stations for a large number of well-recorded earthquakes at Aso volcano, Kyushu, Japan. A low-velocity surface layer with Swave velocity of 2 km/s was required to have the synthetic surface waves propagate at a velocity near 2 km/s. Moderate Q values were assumed (see table 2). We assumed an implosive source with −1 on the diagonal elements of the moment tensor and 0 on the off-diagonal elements. The synthetics were convolved with a triangular source pulse of 1-s duration and then lowpass filtered at 1 Hz.

The synthetic waveforms in figure 11*B* did a reasonable job of predicting the character of the initial arrivals and the beginning of the surface wave train. The synthetic P wave had a down first motion and was emergent at all azimuths. The synthetics do not have the long duration of the observed surface waves but rather a slightly dispersed surface wave traveling at approximately 2 km/s. We also tested other reasonable permutations of the layer velocities within a vertically stratified velocity model without producing the low-frequency coda. From this exercise we concluded that the low-frequency coda observed in figure 11*A* was not produced by a slow surface layer in a 1D velocity model. Scattering of low-frequency surface waves by the extreme local topography of the volcano would be a likely source of some of the coda. The resonance of a source structure (for example, Chouet, 1996, or Neuberg and others, 2006) could also contribute. Examination of surface-wave propagation in a 3D velocity model was beyond the scope of the current study. Unfortunately, we concluded that our simple 1D velocity model was inadequate for modeling waveforms for the purpose of determining the source time function and focal mechanism for these events, because the coda would map into the source.

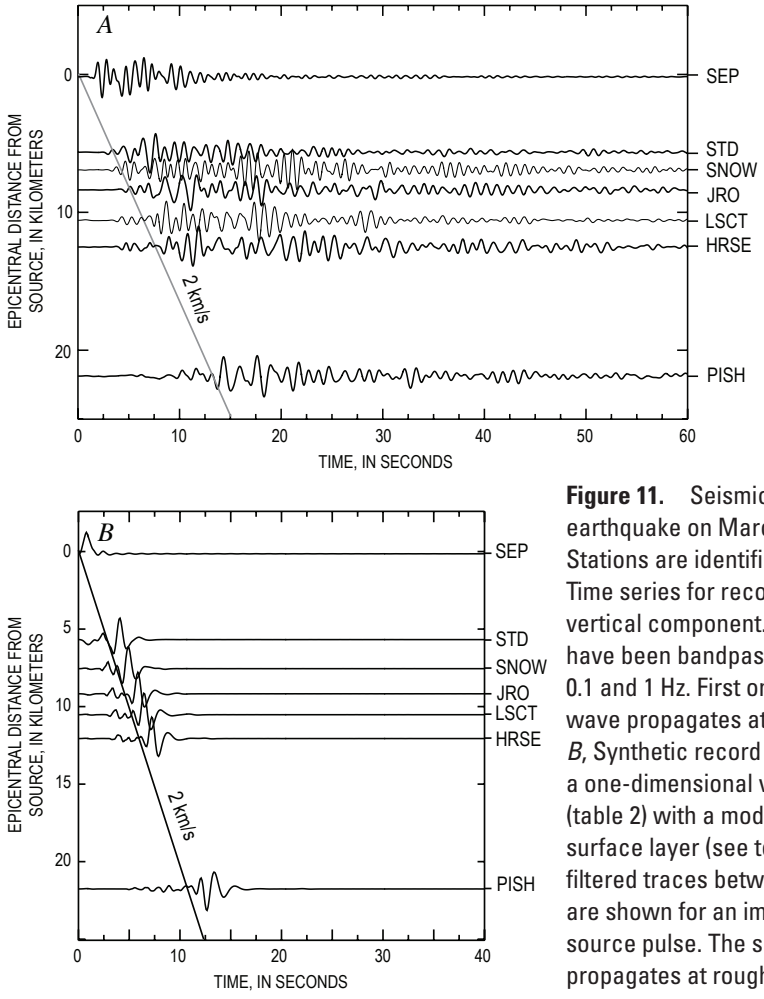

Figure 11. Seismic data for earthquake on March 1, 2005. Stations are identified at right. *A*, Time series for record section from vertical component. Vertical traces have been bandpass filtered between 0.1 and 1 Hz. First onset of the surface wave propagates at roughly 2 km/s. *B*, Synthetic record section assuming a one-dimensional velocity model (table 2) with a moderately slow surface layer (see text). Bandpass-filtered traces between 0.1 and 1 Hz are shown for an implosive, triangular source pulse. The surface wave propagates at roughly 2 km/s.

Table 2. Velocity structure of Mount St. Helens used in this study.

[For a material cycled in stress, Q is the inverse ratio of the energy lost each cycle to the peak strain energy. Q_P and Q_S specify the anelasticity of a material to P- and S-wave motion, respectively.]

Layer	Depth to top of layer (km)	S-wave velocity (km/s)	P-wave velocity (km/s)	Density (g/cm^3)	Q_S	Q_P
1	0	2.0	3.4	2.1	100	200
2	2	3.18	5.4	2.2	100	200
3	4	3.75	6.38	2.2	100	200
4	9	3.88	6.59	2.3	100	200
5	16	3.96	6.73	2.8	250	500
6	20	4.04	6.86	2.8	250	500
7	25	4.09	6.95	2.8	250	500
8	32	4.06	6.90	2.8	250	500
9	41	4.59	7.85	3.3	300	600

Summary

A network of broadband seismometers was rapidly deployed at Mount St. Helens when it became restless in September 2004 and maintained through the winter of 2004–5 without a significant loss of data. A principal reason for deploying broadband seismometers was to record any very long period (VLP) seismicity (5–30 s) associated with the eruption that would otherwise have been missed by the PNSN short-period stations. We found no evidence of VLP pulses at our stations in the first 2 months of recording. Our closest stations were more than 5 km distant from the centroid of seismic activity, and these pulses may attenuate too quickly to be observed at that distance.

More than 57,000 earthquakes were recorded during the 7-month deployment. They had a normal magnitude distribution, with a mean magnitude of 1.78 and a standard deviation of 0.24 magnitude units. Both the mode and range of earthquake size and the rate of activity varied during the 7-month period. Some cases of this variation can be associated with spine growth and breakup. In general, larger earthquakes tended to occur when the earthquake rate was high.

The dataset consisted largely of hybrid and low frequency (LF) earthquakes. These lower-frequency events typically had a low amplitude onset with frequencies up to about 10 or 20 Hz, followed by a strong, long-duration, and lower-frequency waveform. The shape of the Fourier spectrum at the low-frequency end was similar for both types of events, having significant energy between 0.3 and 5 Hz with multiple spectral peaks. Hybrid events exhibited more energetic high-frequency onsets than LF events, but the rate of high-frequency decay with time was similar for both types. The difference in high-frequency energy was more likely related to the source than to attenuation near the source or along the path, inasmuch as the high-frequency decay rate was the same for both events.

The spectra of large and small events that occurred close in time were quite similar in shape between 0.5 and 10 Hz. The similarity in spectral shape suggested that both the source and path were similar for the larger and smaller events. As opposed to the ideal tectonic earthquake spectra, in which the peak in the velocity spectrum changes to lower frequency as rupture zone area increases for larger earthquakes, the frequency range of the peak of spectral energy remained constant for different-size, lower-frequency earthquakes. This relative constancy is consistent with a resonating source, whereby the shape of the spectrum is constrained by the size and properties of the resonator. However, a search of spectra of the same events observed at multiple stations revealed no specific frequencies of source resonance, and so the spectra may reflect a complex, perhaps asymmetric, resonating structure.

The spectra of a lower-frequency earthquake and an episode of volcanic tremor had distinct peaks in common. However, the lower-frequency earthquake spectrum had a prominent peak at 0.6 Hz that was not observed in the spectrum of the volcanic tremor, and higher frequencies were more favorably excited during the tremor. This lower-frequency peak would be consistent with resonance of a larger structure during the earthquake or a change in the source such that excitation of the longer dimension of the same structure was favorable.

The high-frequency spectral difference between hybrid and LF events was quantified using the slope of the high-frequency falloff. The slope computed for several thousand lower-frequency earthquakes between October 4 and December 1, 2004, defined a continuum between the ideal hybrid and ideal LF events. The slope started relatively high on October 4 and transitioned smoothly to lower values until around October 14. The gradual decrease in the slope of the high-frequency falloff over time reflected a progressive loss of high-frequency seismic energy as magma approached and eventually reached the surface.

The first onset of the surface-wave train produced by low-frequency earthquakes propagated at roughly 2 km/s. This propagation velocity favors an areally extensive surface layer with an average S-wave velocity of about 2 km/s. A window of the vertical and radial components for a 2 km/s group velocity has retrograde elliptical particle motion when observed at 20 km distance. Signal duration ranges from 15 to 50 s. A one-dimensional velocity model was unsuitable for waveform modeling to determine the source time function and focal mechanism of the lower-frequency earthquakes.

Acknowledgments

Deployment and maintenance of the seismic network was facilitated by numerous individuals at the U.S. Forest Service, the Cascades Volcano Observatory, and the Pacific Northwest Seismic Network of the University of Washington. Federal Express shipped our equipment to Portland, Oregon, without cost. We are grateful to Thomas Brackman, Chris Watson,

and Gary Patterson of the Center for Earthquake Research and Information (CERI) at the University of Memphis for taking time to assist in the field. We obtained seismic data for stations LON, JRO, and STD from the Incorporated Research Institutions for Seismology Data Management Center. Greg Waite and Charles Langston provided thoughtful and helpful reviews of this paper. This is CERI contribution 511.

References Cited

Almendros, J., and Chouet, B., 2003, Performance of the radial semblance method for the location of very long period volcanic signals: Seismological Society of America Bulletin, v. 93, p. 1890–1903.

Almendros, J., Chouet, B., Dawson, P., and Bond, T., 2002, Identifying elements of the plumbing system beneath Kilauea Volcano, Hawaii, from the source locations of very-long-period signals: Geophysical Journal International, v. 148, p. 303–312.

Aster, R., Mah, S., Kyle, P., McIntosh, W., Dunbar, N., Johnson, J., Ruiz, M., and McNamara, S., 2003, Very long period oscillations of Mount Erebus Volcano: Journal of Geophysical Research, v. 108, no. B11, 2522, doi:10.1029/2002JB002101.

Brune, J.N., 1970, Tectonic stress and the spectra of seismic shear waves from earthquakes: Journal of Geophysical Research, v. 75, no. 23, p. 4997–5009.

Chouet, B.A., 1996, Long-period volcano seismicity; its source and use in eruption forecasting: Nature, v. 380, p. 309–316.

Endo, E.T., Malone, S.D., Noson, L.L., and Weaver, C.S., 1981, Locations, magnitudes, and statistics of the March 20–May 18 earthquake sequence, *in* Lipman, P.W., and Mullineaux, D.R., eds., The 1980 eruptions of Mount St. Helens, Washington: U.S. Geological Survey Professional Paper 1250, p. 93–107.

Fehler, M., 1983, Observations of volcanic tremor at Mount St. Helens Volcano: Journal of Geophysical Research: v. 88, p. 3476–3484.

Lahr, J.C., Chouet, B.A., Stephens, C.D., Power, J.A., and Page, R.A., 1994, Earthquake classification, location, and tremor analysis in a volcanic environment; implications for the magmatic system of the 1989–1990 eruptions at Redoubt Volcano, Alaska: Journal of Volcanology and Geothermal Research, v. 62, nos. 1–4, p. 137–151, doi:10.1016/0377-0273(94)90031-0.

Latter, J.H., 1981, Volcanic earthquakes, and their relationship to eruptions at Ruapehu and Ngauruhoe volcanoes: Journal of Volcanology and Geothermal Research, v. 9, p. 293–309.

Lees, J.M., and Crosson, R.S., 1989, Tomographic inversion for three-dimensional velocity structure at Mount St. Helens using earthquake data: Journal of Geophysical Research, v. 94, no. B5, p. 5716–5728.

Longuet-Higgins, M.S., 1950, A theory of the origin of microseisms: Philosophical Transactions of the Royal Society of London, series A, v. 243, p. 1–35.

Malone, S.D., 1983, Volcanic earthquakes; examples from Mount St. Helens, *in* Earthquakes; observations, theory and interpretation: Bologna, Italy, Società Italiana di Fisica, p. 436–455.

Malone, S.D., Boyko, C., and Weaver, C.S., 1983, Seismic precursors to the Mount St. Helens eruptions in 1981 and 1982: Science, v. 221, p. 1376–1378.

McChesney, P.J., Couchman, M.R., Moran, S.C., Lockhart, A.B., Swinford, K.J., and LaHusen, R.G., 2008, Seismic-monitoring changes and the remote deployment of seismic stations (seismic spider) at Mount St. Helens, 2004–2005, chap. 7 *of* Sherrod, D.R., Scott, W.E., and Stauffer, P.H., eds., A volcano rekindled; the renewed eruption of Mount St. Helens, 2004–2006: U.S. Geological Survey Professional Paper 1750 (this volume).

Moran, S.C., Malone, S.D., Qamar, A.I., Thelen, W.A., Wright, A.K., and Caplan-Auerbach, J., 2008a, Seismicity associated with renewed dome building at Mount St. Helens, 2004–2005, chap. 2 *of* Sherrod, D.R., Scott, W.E., and Stauffer, P.H., eds., A volcano rekindled; the renewed eruption of Mount St. Helens, 2004–2006: U.S. Geological Survey Professional Paper 1750 (this volume).

Moran, S.C., McChesney, P.J., and Lockhart, A.B., 2008b, Seismicity and infrasound associated with explosions at Mount St. Helens, 2004–2005, chap. 6 *of* Sherrod, D.R., Scott, W.E., and Stauffer, P.H., eds., A volcano rekindled; the renewed eruption of Mount St. Helens, 2004–2006: U.S. Geological Survey Professional Paper 1750 (this volume).

Neuberg, J., Luckett, R., Baptie, B., and Olsen, K., 2000, Models of tremor and low-frequency earthquake swarms on Montserrat: Journal of Volcanology and Geothermal Research, v. 101, p. 83–104.

Neuberg, J.W., Tuffen, H., Collier, L., Green, D., Powell, T., and Dingwell, D., 2006, The trigger mechanism of low-frequency earthquakes on Montserrat: Journal of Volcanology and Geothermal Research, v. 153, nos. 1–2, p. 37–50, doi:10.1016/j.jvolgeores.2005.08.008.

Randall, G.R., Ammon, C.J., and Owens, T.J., 1995, Moment-tensor estimation using regional seismograms from a Tibetan Plateau portable network deployment: Geophysical Research Letters, v. 22, p. 1665–1668.

Schilling, S.P., Thompson, R.A., Messerich, J.A., and Iwatsubo, E.Y., 2008, Use of digital aerophotogrammetry to

determine rates of lava dome growth, Mount St. Helens, Washington, 2004–2005, chap. 8 *of* Sherrod, D.R., Scott, W.E., and Stauffer, P.H., eds., A volcano rekindled; the renewed eruption of Mount St. Helens, 2004–2006: U.S. Geological Survey Professional Paper 1750 (this volume).

Scott, W.E., Sherrod, D.R., and Gardner, C.A., 2008, Overview of 2004 to 2006, and continuing, eruption of Mount St. Helens, Washington, chap. 1 *of* Sherrod, D.R., Scott, W.E., and Stauffer, P.H., eds., A volcano rekindled; the renewed eruption of Mount St. Helens, 2004–2006: U.S. Geological Survey Professional Paper 1750 (this volume).

Sudo, Y., and Kong, L.S.L., 2001, Three-dimensional seismic velocity structure beneath Aso Volcano, Kyushu, Japan: Bulletin of Volcanology, v. 63, p. 326–344.

Swanson, D.A., Casadevall, T.J., Dzurisin, D., Malone, S.D., Newhall, C.G., and Weaver, C.S., 1983, Predicting eruptions at Mount St. Helens, June 1980 through December 1982: Science, v. 221, no. 4618, p. 1369–1376.

Swanson, D.A., Casadevall, T.J., Dzurisin, D., Malone, S.D., Holcomb, R.T., Newhall, C.G., and Weaver, C.S., 1985, Forecasts and predictions of eruptive activity at Mount St. Helens, USA: 1975–1984: Journal of Geodynamics, v. 3, p. 397–423.

Thelen, W.A., Crosson, R.S., and Creager, K.C., 2008, Absolute and relative locations of earthquakes at Mount St. Helens, Washington, using continuous data; implications for magmatic processes, chap. 4 *of* Sherrod, D.R., Scott, W.E., and Stauffer, P.H., eds., A volcano rekindled; the renewed eruption of Mount St. Helens, 2004–2006: U.S. Geological Survey Professional Paper 1750 (this volume).

Vallance, J.W., Schneider, D.J., and Schilling, S.P., 2008, Growth of the 2004–2006 lava-dome complex at Mount St. Helens, Washington, chap. 9 *of* Sherrod, D.R., Scott, W.E., and Stauffer, P.H., eds., A volcano rekindled; the renewed eruption of Mount St. Helens, 2004–2006: U.S. Geological Survey Professional Paper 1750 (this volume).